Supplementary information

MoO_x-incorporated RuAu composite electrocatalyst for hydrogen evolution reaction for proton exchange membrane water electrolysis

*Jaewon Lee,[ab] Jinho Oh,[ab] Jun Hyeong Kim,[a] Hee-Young Park,[a] Sung Jong Yoo,[a] Hyung-Kyu Lim,[c] Jong Hyun Jang,[*abd] Hyun S. Park,[*ab] Sung Ki Cho,[*a]*

[a]Center for Hydrogen and Fuel Cells, Korea Institute of Science and Technology (KIST), Seoul 02792, Republic of Korea

[b]Division of Energy & Environment Technology, KIST School, University of Science and Technology (UST), Seoul, 02792, Republic of Korea

[c]Division of Chemical Engineering and Bioengineering, Kangwon National University, Chuncheon 24341, Republic of Korea

[d]Graduate School of Energy and Environment, KU-KIST Green School, Korea University, Seoul 02841, Republic of Korea

***Corresponding author (Jong Hyun Jang).** E-mail: : jhjang@kist.re.kr, Tel: +82-2-958-5287

***Corresponding author (Hyun S. Park).** E-mail: hspark@kist.re.kr, Tel: +82-2-958-5250

***Corresponding author (Sung Ki Cho).** E-mail: skcho@kist.re.kr, Tel: +82-2-958-5214

ADDITIONAL INFORMATION

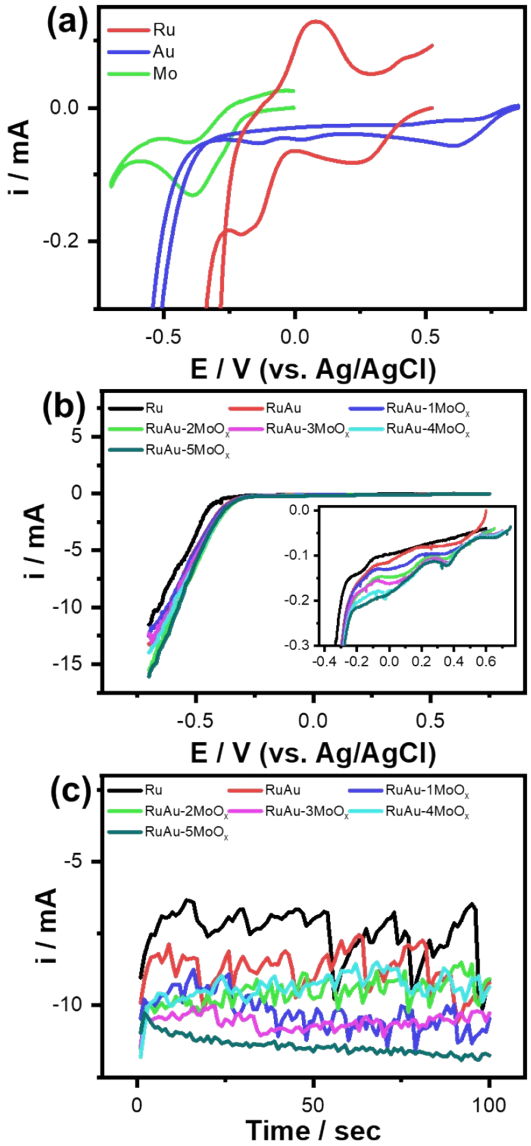

Fig. S1. (a) Cyclic voltammograms for 250 mM $HClO_4$ solution containing 20 mM of $RuCl_3$, $HAuCl_4$, and Na_2MoO_4, respectively. (b) Cyclic voltammograms for the electrolyte for the electrodeposition of RuAu-MoO_x with various Mo concentrations. (c) i-t curve at -0.55 V (vs. Ag/AgCl (KCl sat'd)) for the electrodeposition of RuAu-MoO_x with various Mo concentrations. It is noted that, in Fig. S1a, the small reduction current emerging at 0.4 V (vs. Ag/AgCl) was attributed to Ru at higher intermediate valence state, which was generated near the electrode.[1]

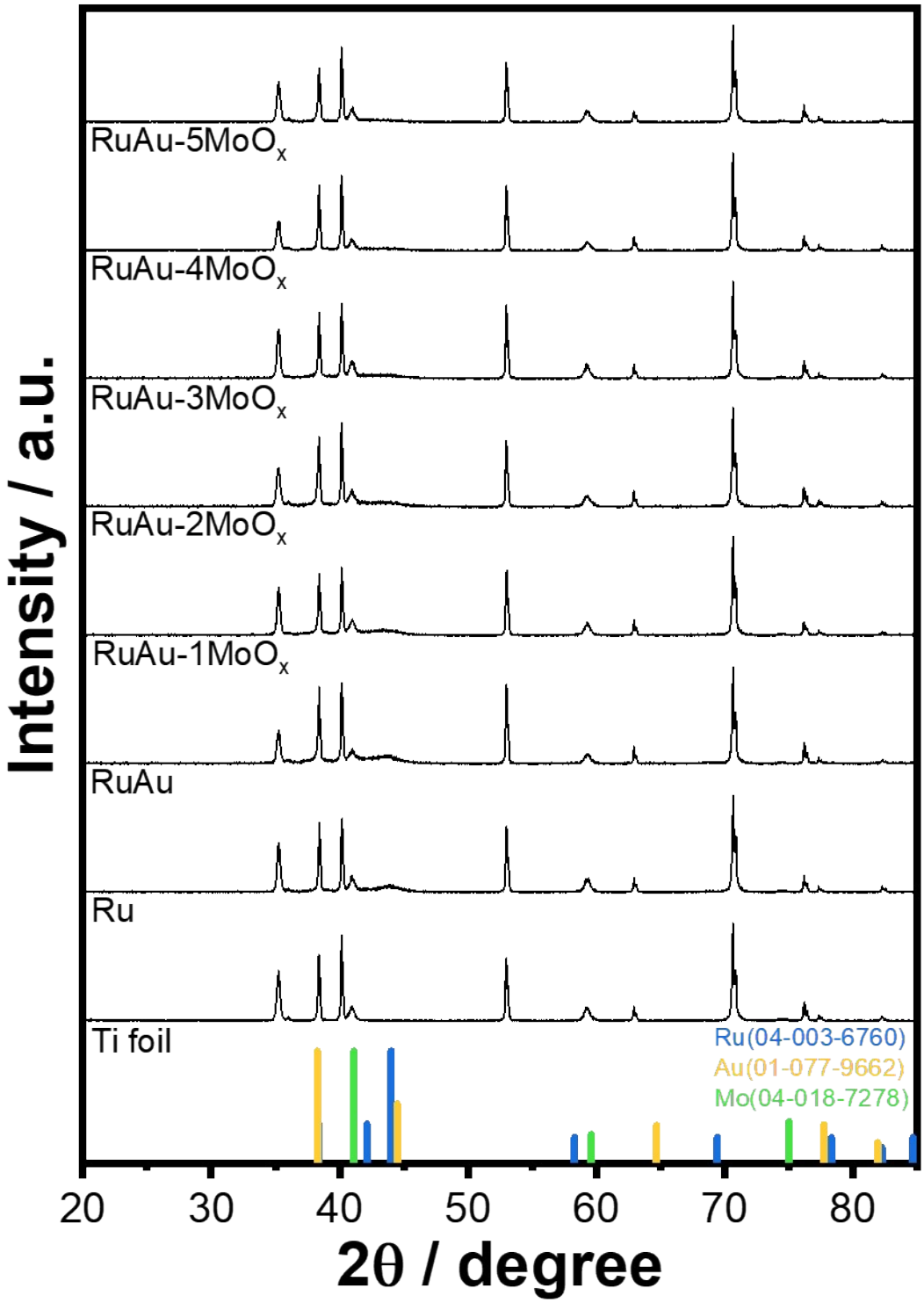

Fig. S2. X-ray diffraction patterns of Ru, RuAu, RuAu-1–5MoO_x deposits on Ti foil and bare Ti foil.

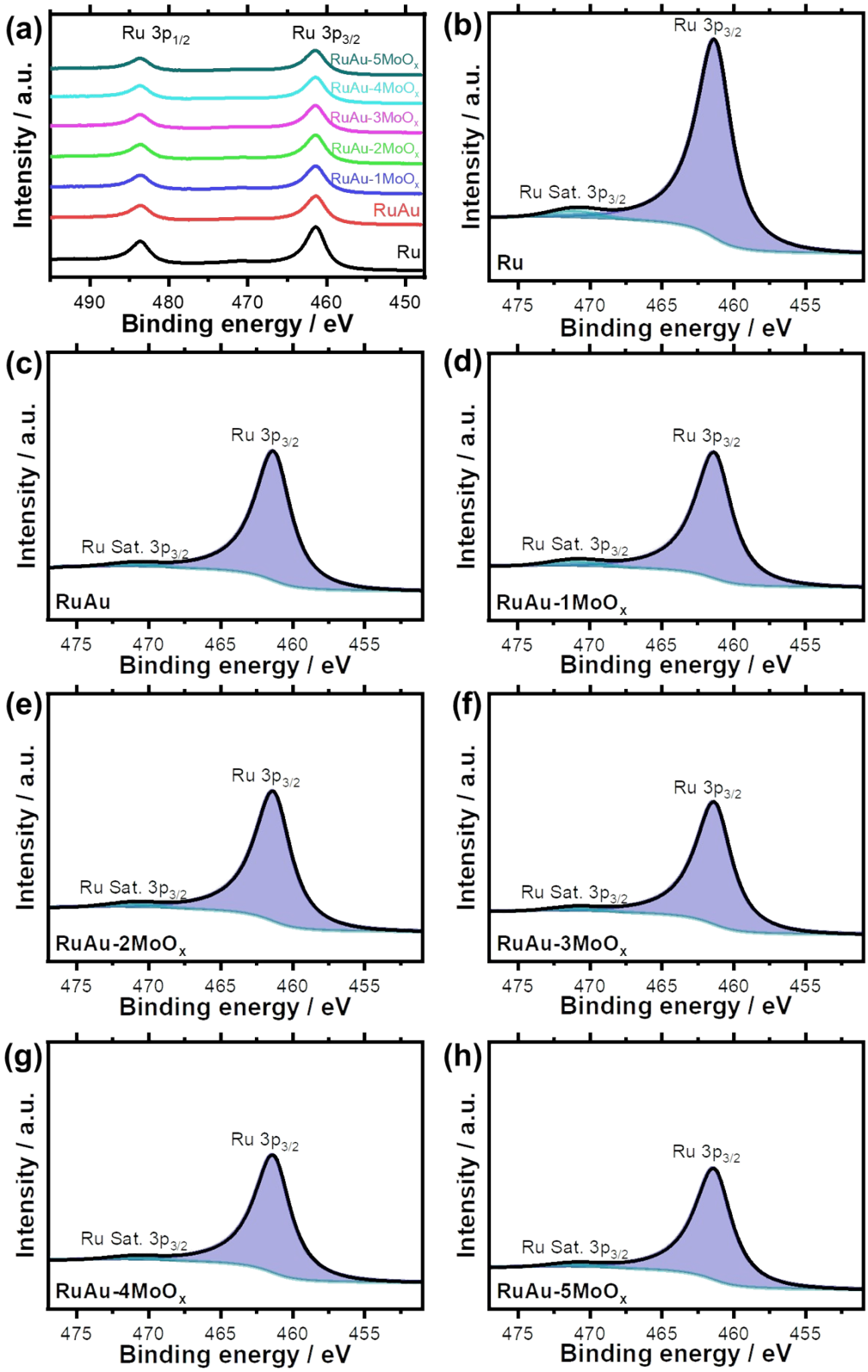

Fig. S3. Ru 3p XPS spectra of (a) all deposits, (b) Ru, (c) RuAu, (d–h) RuAu-1–5MoO_x deposits on Ti foil.

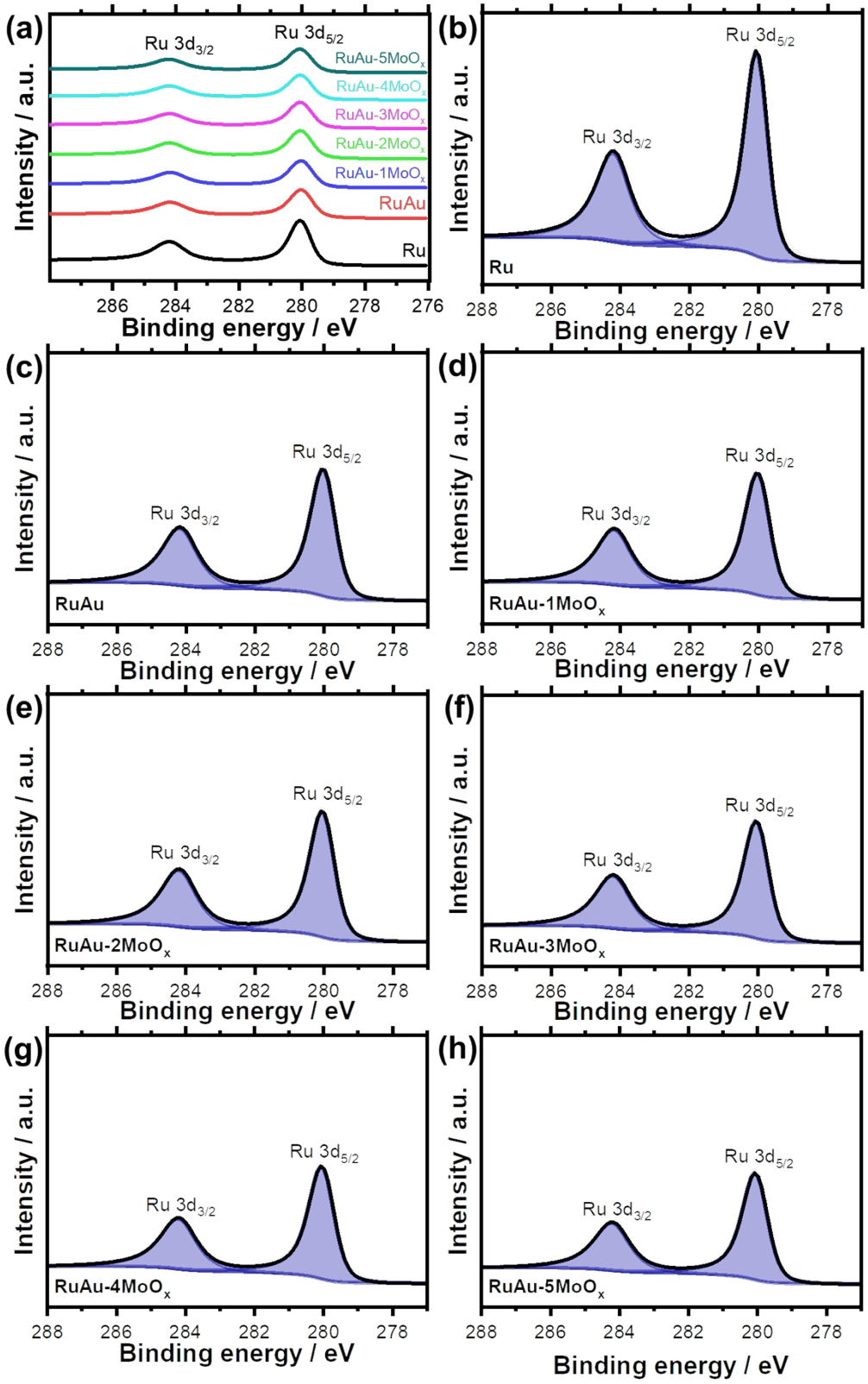

Fig. S4. Ru 3d XPS spectra of (a) all deposits, (b) Ru, (c) RuAu, (d–h) RuAu-1–5MoO_x deposits on Ti foil.

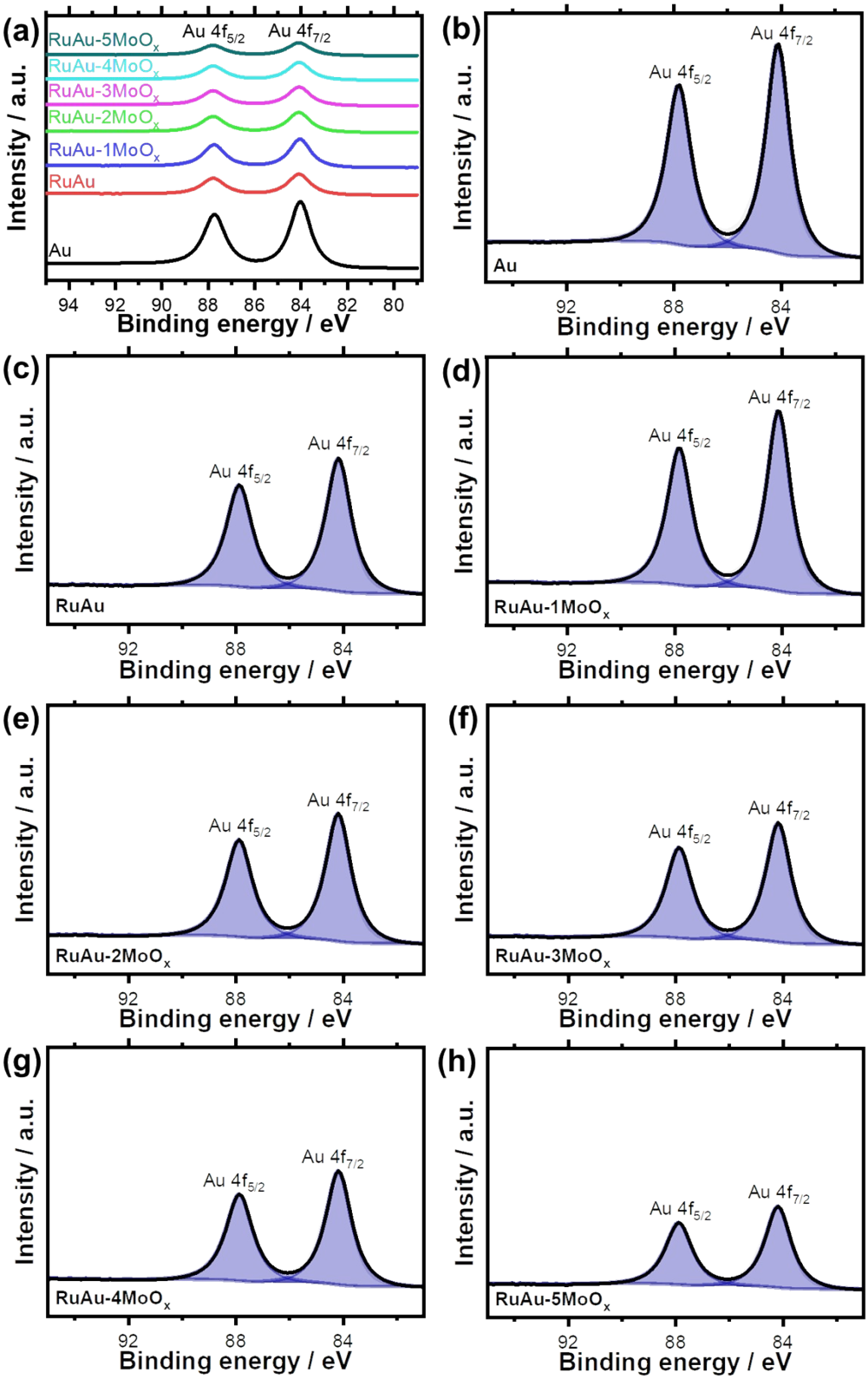

Fig. S5. Au 4f XPS spectra of (a) all deposits, (b) Au, (c) RuAu, (d–h) RuAu-1–5MoO_x deposits on Ti foil.

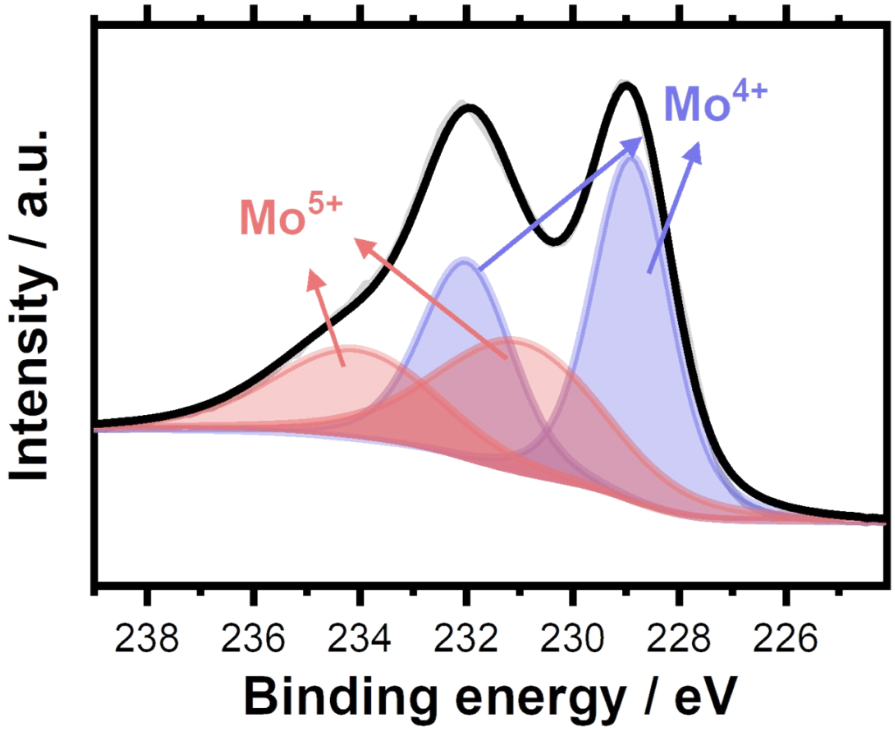

Fig. S6. Mo 3d XPS spectrum of Mo deposit on Ti foil.

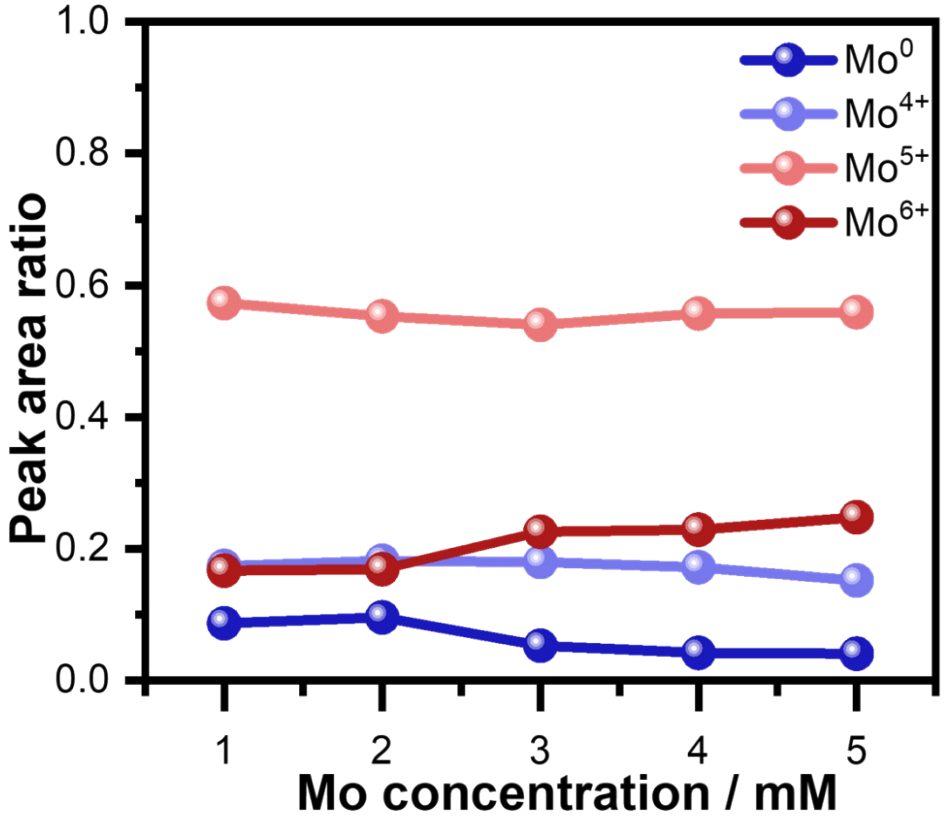

Fig. S7. Peak area ratios of deconvoluted Mo 3d XPS spectra for RuAu-1–5MoO_x deposits.

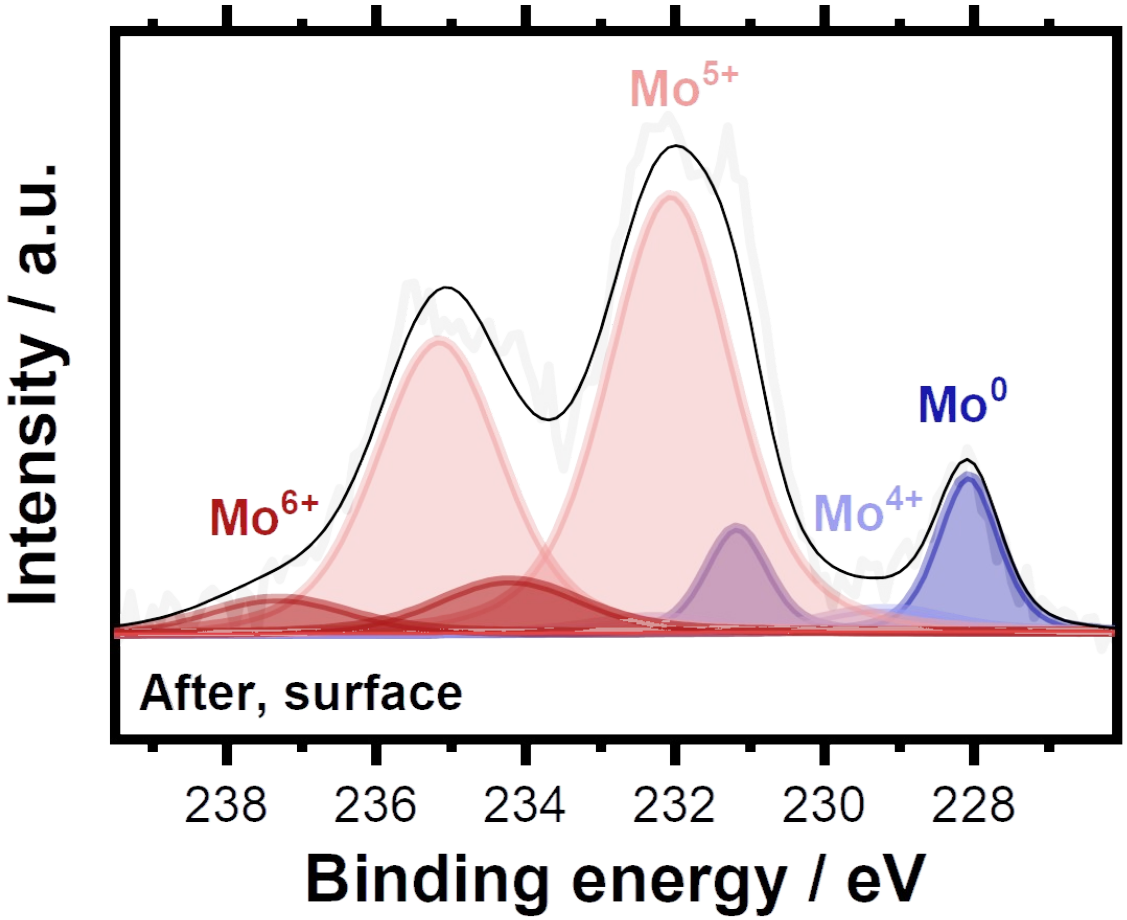

Fig. S8. Mo 3d spectrum of RuAu-2MoO_x after HER (at -50 mA·cm^{-2} for 4 hours).

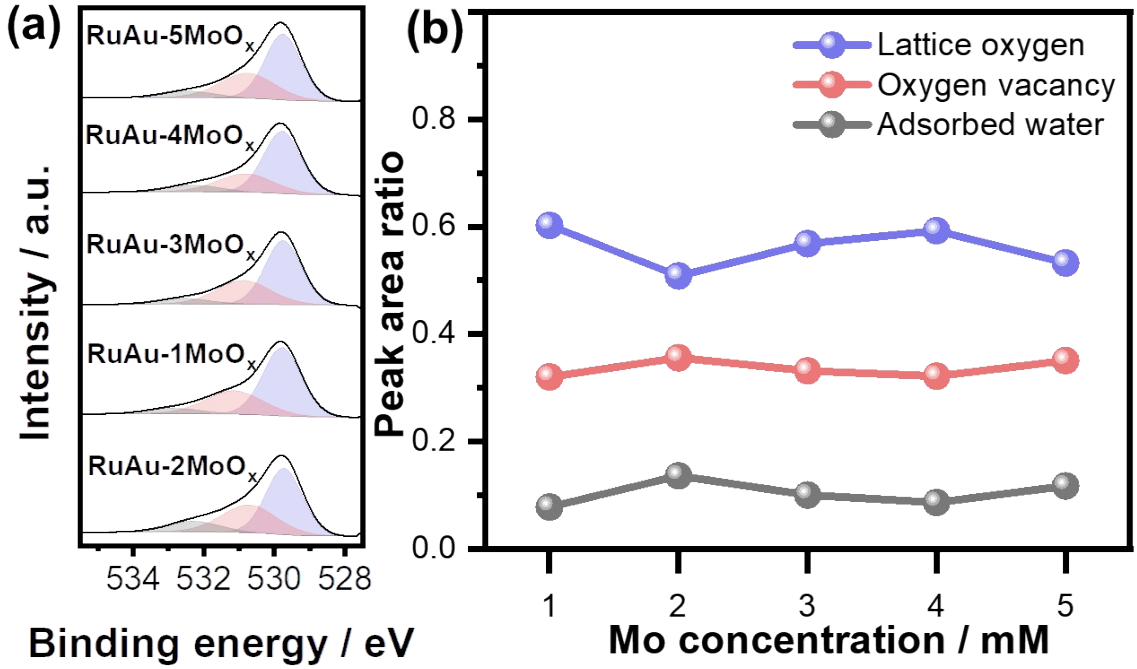

Fig. S9. (a) O 1s spectra of RuAu-1–5MoO_x deposits on Ti foil and (b) the corresponding peak area ratios of deconvoluted O 1s XPS spectra.

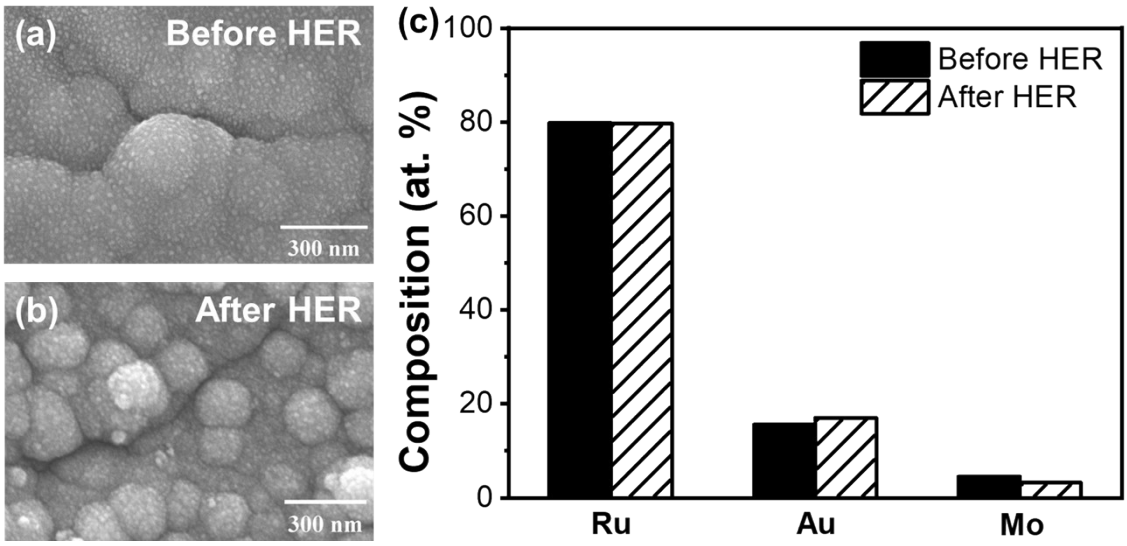

Fig. S10. Top view SEM images of RuAu-2MoOx (a) before and (b) after HER (at -10 mA·cm^{-2} for 48 hr) and (c) their atomic compositions (obtained from EDS analysis).

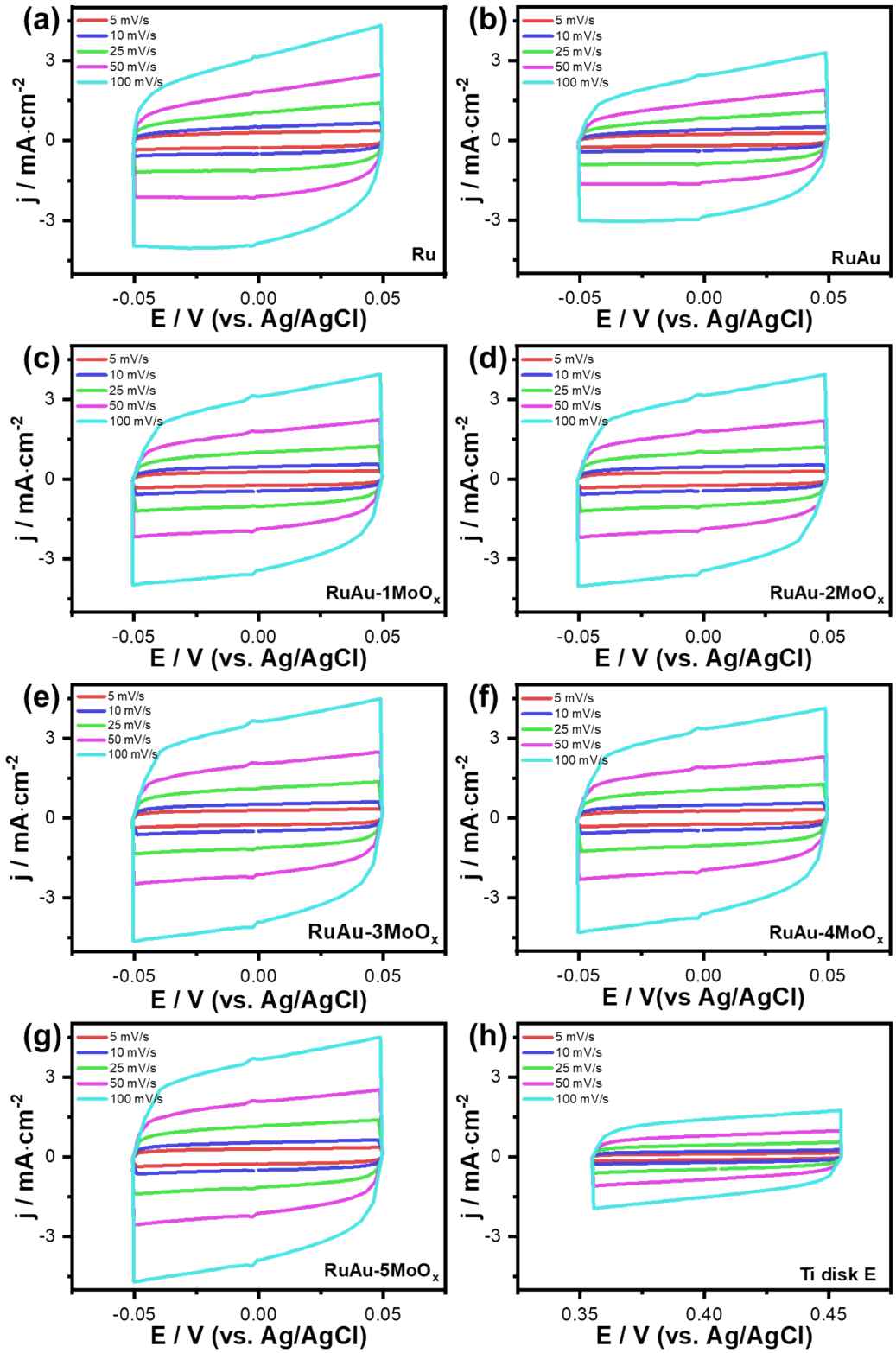

Fig. S11. Cyclic voltammograms (scan rate: 5, 10, 25, 50, 100 mV/s) for (a) Ru, (b) RuAu, (c–g) RuAu-1–5MoO_x deposits on Ti RDE and (h) bare Ti RDE.

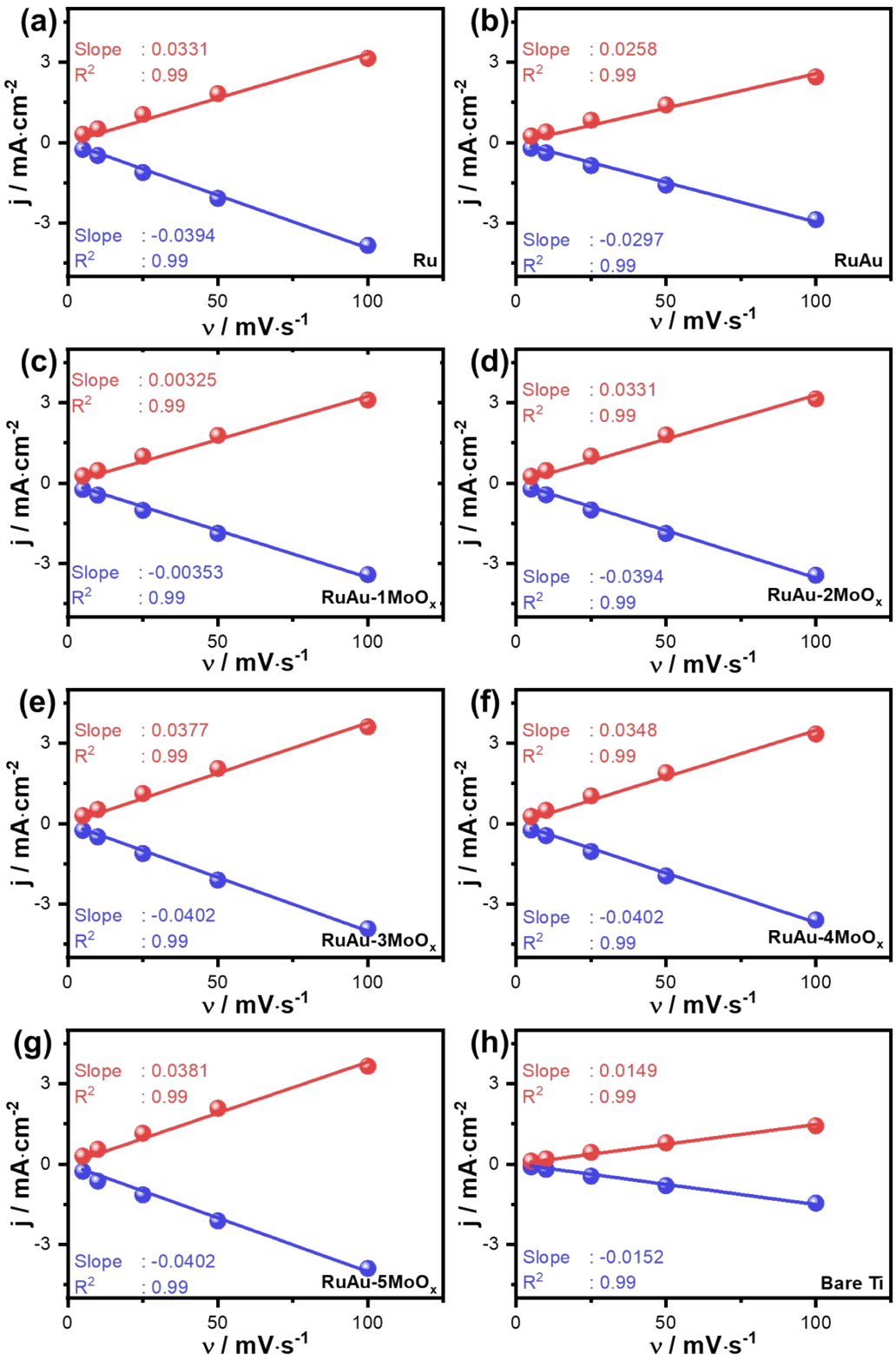

Fig. S12. Plots of double-layer charging current density vs. scan rates for (a) Ru, (b) RuAu, (c–g) RuAu-1–5MoO_x deposits on Ti RDE and (h) bare Ti RDE.

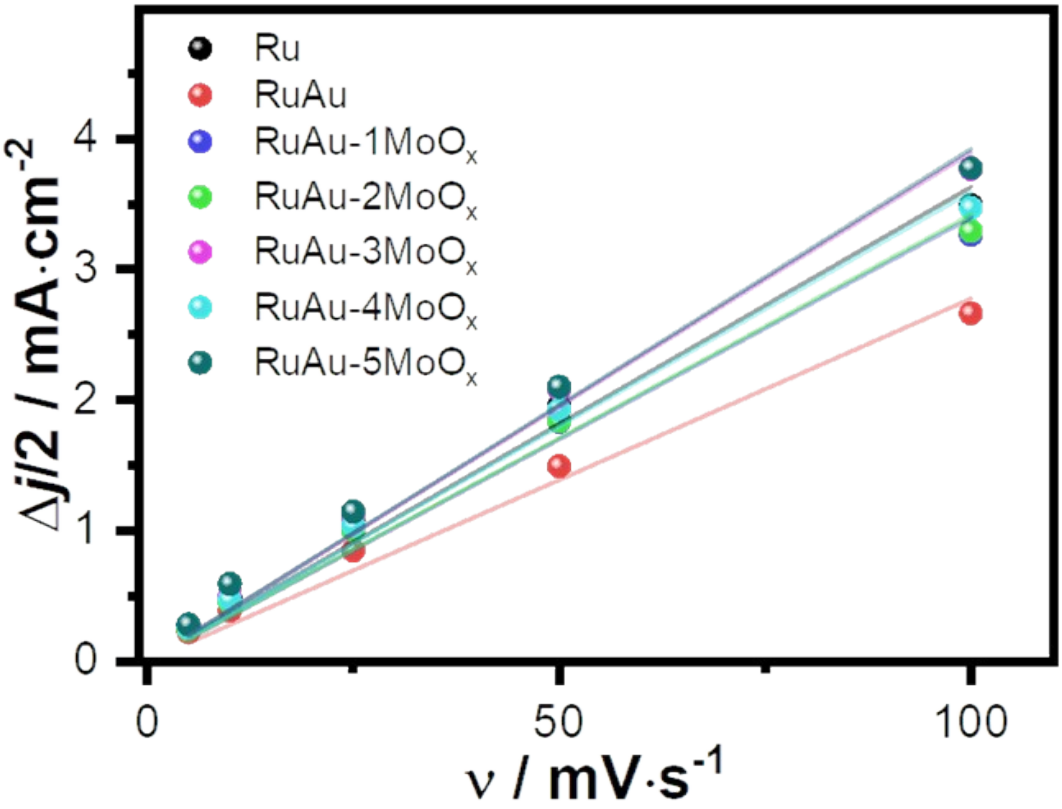

Fig. S13. Comparison of double-layer capacitance based on the slopes obtained from plots of double-layer charging current density vs. scan rates.

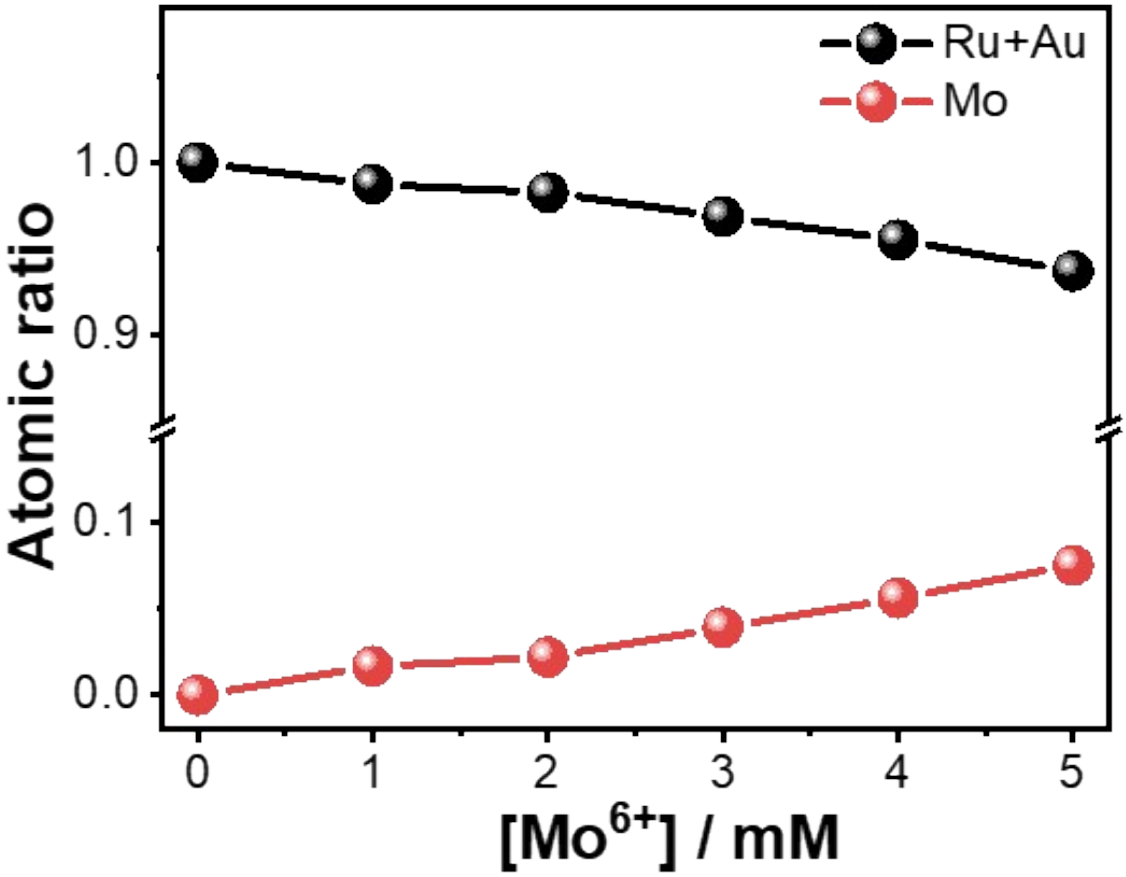

Fig. S14. The Atomic ratio of Mo with respect to RuAu according to the Mo precursor concentration, calculated from XPS signals.

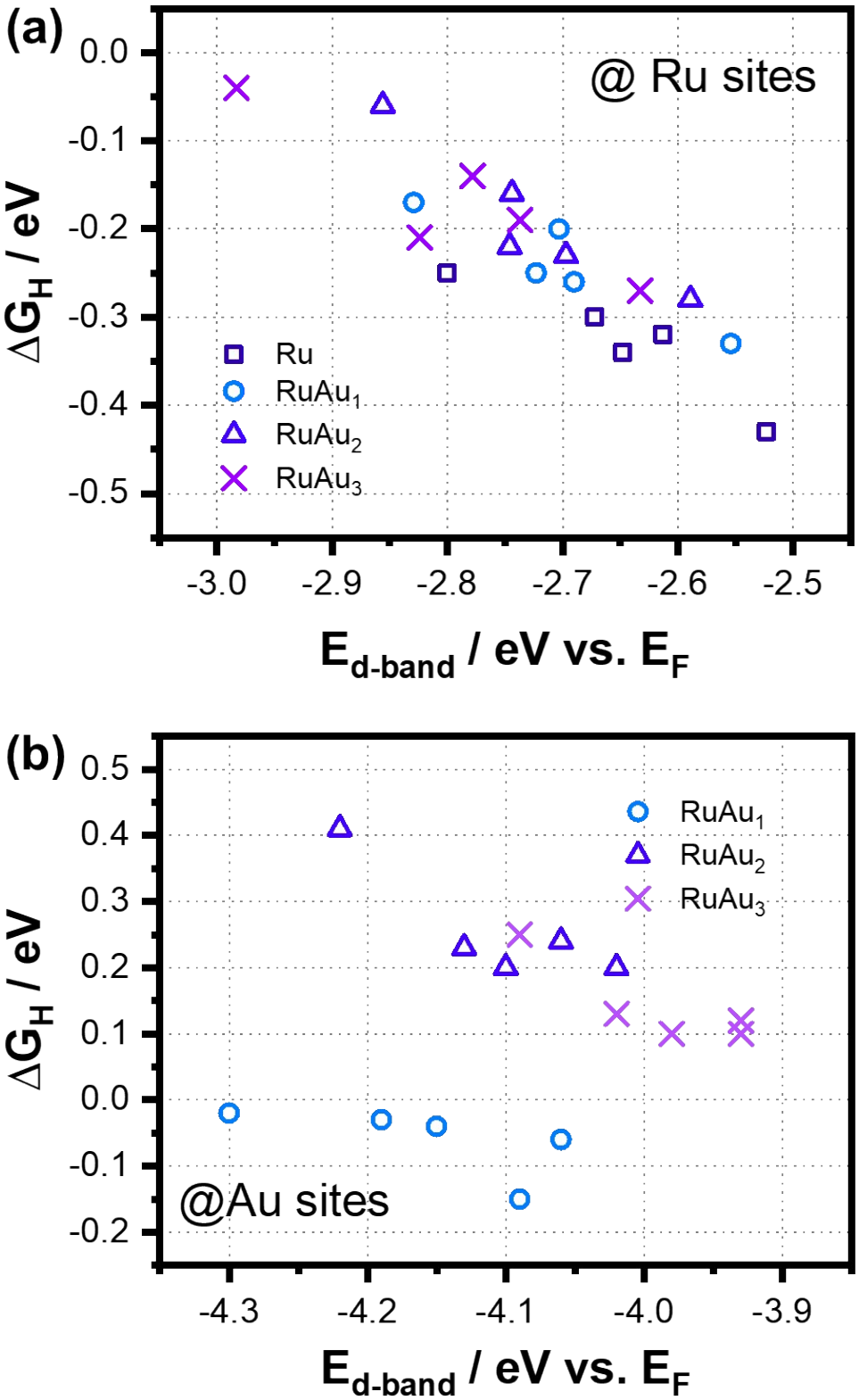

Fig. S15. Correlation between *d*-band center of surface metals and hydrogen binding free energy (ΔG_H) for (a) Ru sites and (b) Au sites in various RuAu-MoO_x catalyst models.

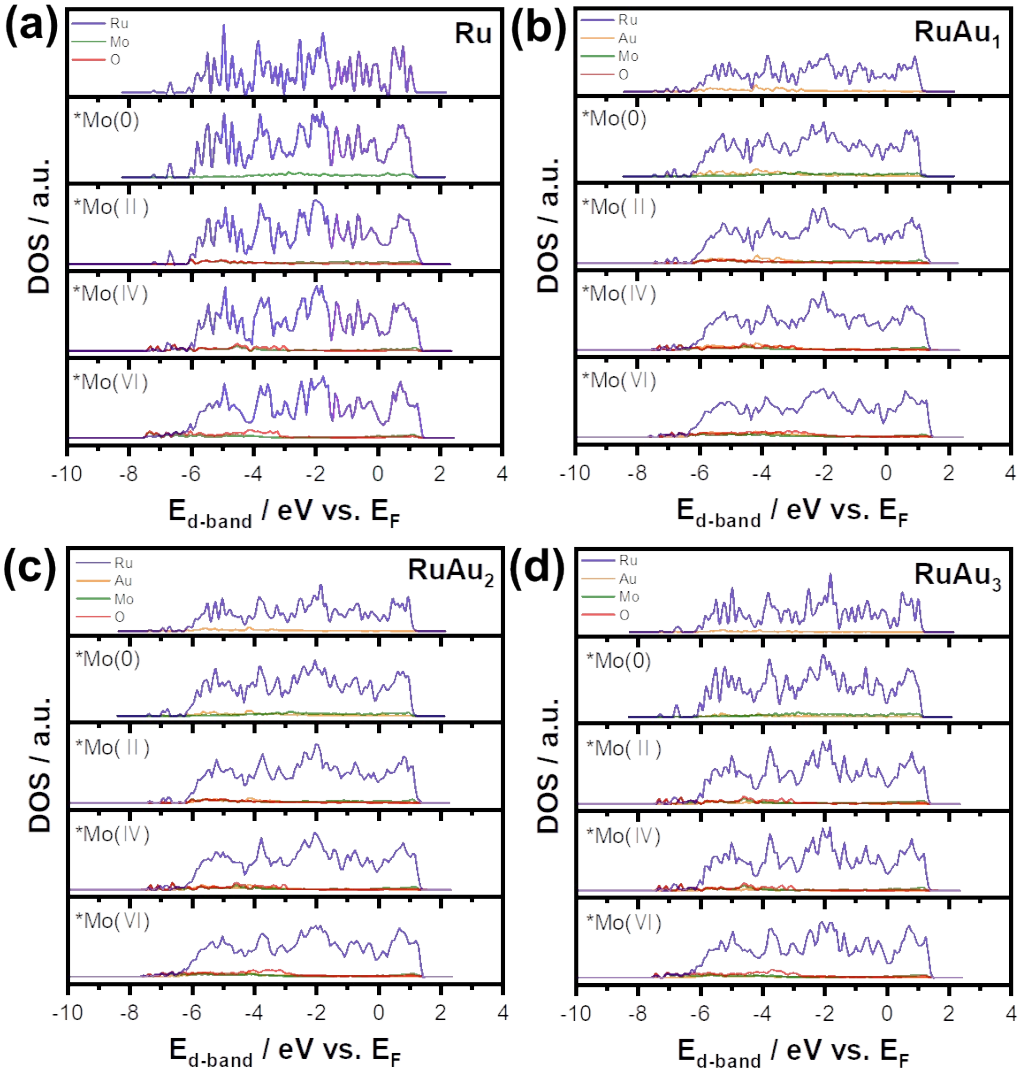

Fig. S16. Projected density of states (PDOS) for (a) Ru, (b) $RuAu_1$, (c) $RuAu_2$, and (d) $RuAu_3$ surfaces with varying MoO_x oxidation states.

Table S1. Nomenclature of each metal deposits defined in terms of concentration of metal precursors dissolved in solution.

Nomenclature	**Ru**	**RuAu**	**RuAu-1MoO$_x$**	**RuAu-2MoO$_x$**	**RuAu-3MoO$_x$**	**RuAu-4MoO$_x$**	**RuAu-5MoO$_x$**
$RuCl_3$ (mM)	20	20	20	20	20	20	20
$HAuCl_4$ (mM)	0	1	1	1	1	1	1
Na_2MoO_4 (mM)	0	0	1	2	3	4	5
$HClO_4$ (mM)	250	250	250	250	250	250	250

Table S2. Atomic concentration of each metals investigated by EDS (FE-SEM) with the change in the concentration of Mo precursor in electrodeposition process.

At. % (SEM-EDS)	Ru	RuAu	RuAu-1MoO$_x$	RuAu-2MoO$_x$	RuAu-3MoO$_x$	RuAu-4MoO$_x$	RuAu-5MoO$_x$
Ru	100	87.8	82.4	79.8	79.6	78.2	77.7
Au	0	12.2	13.9	15.6	15.2	15.7	15.8
Mo	0	0	3.7	4.6	5.2	6.1	6.5

Table S3. Calculated lattice distance and crystal size of each metal deposits.

Thin-film XRD	**Ru**	**RuAu**	**RuAu-1MoO$_x$**	**RuAu-2MoO$_x$**	**RuAu-3MoO$_x$**	**RuAu-4MoO$_x$**	**RuAu-5MoO$_x$**
d-spacing (nm)	0.2071	0.2081	0.2085	0.2084	0.2089	0.2087	0.2096
Crystal size (nm)	6.8742	6.7286	6.1108	7.0690	6.6642	5.4239	4.8841

Table S4. HER overpotentials at current density of -10 mA·cm^{-2}, Tafel slopes of Ru, RuAu, RuAu-1–5MoO$_x$ deposited on Ti RDE.

Catalyst	**Ru**	**RuAu**	**RuAu-1MoO$_x$**	**RuAu-2MoO$_x$**	**RuAu-3MoO$_x$**	**RuAu-4MoO$_x$**	**RuAu-5MoO$_x$**	**Pt/C**
Overpotential (mV@ -10 mA·cm^{-2})	71.3	41.2	35.8	34.1	35.7	38.3	39.2	20
Tafel slope (mV·decade^{-1})	43.9± 0.48	40.8± 0.46	38.1± 0.21	38.7± 0.25	38.8± 0.17	38.8± 0.18	40.2± 0.11	45.3± 0.2

Table. S5. Electrochemical impedance spectroscopy (EIS) fitting data corresponding to Fig. 4d.

	Ru	**RuAu**	**RuAu-2MoO$_x$**	**RuAu-5MoO$_x$**
R_{ohm} (ohm)	4.88	7.79	6.70	8.59
R_{ct} (ohm)	35.21	10.61	10.27	12.32
C_{dl} (F)	$0.475 \cdot 10^{-3}$	$11.24 \cdot 10^{-3}$	$19.1 \cdot 10^{-3}$	$14.46 \cdot 10^{-3}$
Z_w (ohm·s$^{-1/2}$)	15.29	0.449	0.428	0.716

Table S6. Relative surface area (vs. RuAu) in terms of amounts of Mo precursor added in solution for electrodeposition.

Mo conc.	**0**	**1**	**2**	**3**	**4**	**5**
$C_{dl,avg}$ ($mF \cdot cm^{-2}$)	27.8	33.9	34.2	38.9	35.9	39.2
Relative area (vs. RuAu)	1	1.22	1.23	1.40	1.29	1.41

Table S7. Summary of PEMWE operation conditions of recently reported literatures.

	Cathode ($mg \cdot cm^{-2}$)	Anode ($mg \cdot cm^{-2}$)	Membrane	T (°C)	j@1.8 V ($A \cdot cm^{-2}$)
This work	RuAu-2MoO_x (0.19)	Pt@IrO_2 (0.43)	NR212	80	2.48
Ref.[2]	CoRu alloy (0.248)	IrO_2 (0.1)	NR212	90	1.49
Ref.[3]	$Ni_{98.1}Ru_{1.9}$ (1.396)	IrO_x (2)	NR212	90	1.32
Ref.[4]	RuP (0.8)	Ir black (1)	NR212	80	1.03
Ref.[5]	RuP/NPC (0.87)	IrRuPt (3)	-	50	0.87
Ref.[6]	Ru/Ti_4O_7 (0.96)	Ru/Ti_4O_7 (2)	NR117	80	0.96
Ref.[7]	$RuTe_2$ (2)	IrO_2 (2.5)	Gore M820.15	80	0.69
Ref.[8]	Ru_3Mo (4.5)	IrO_2 (2.5)	NR212	80	0.56

Supplementary References

1. R. Zou, Y. Wang, M. Hu, Y. Wei and T. Fujita, J. Phys. Chem. C, 2022, 126, 4329-4337.
2. T. Lee, Y. Park, H. Kim, Y. K. Hong, E. Hwang, M. Kim, S. K. Kim and D. H. Ha, Int. J. Energy Res., 2022, 46, 7975-7987.
3. K.-R. Yeo, H. Kim, K.-S. Lee, S. Kim, J. Lee, H. Park and S.-K. Kim, Appl. Catal. B-Environ. Energy, 2024, 346, 123738.
4. D. Galyamin, J. Torrero, J. D. Elliott, I. Rodríguez-García, D. G. Sánchez, M. A. Salam, A. S. Gago, M. Mokhtar, J. L. Gómez de la Fuente and S. V. Bueno, Adv. Energy Sustain. Res., 2023, 4, 2300059.
5. R. Ma, Y. Wang, G. Li, L. Yang, S. Liu, Z. Jin, X. Zhao, J. Ge and W. Xing, Nano Res., 2021, 14, 4321-4327.
6. S. Zhao, S.-F. Hung, L. Deng, W.-J. Zeng, T. Xiao, S. Li, C.-H. Kuo, H.-Y. Chen, F. Hu and S. Peng, Nat. Commun., 2024, 15, 2728.
7. Z. Zhang, C. Jiang, P. Li, K. Yao, Z. Zhao, J. Fan, H. Li and H. Wang, Small, 2021, 17, 2007333.
8. Z. Zhang, P. Li, Q. Wang, Q. Feng, Y. Tao, J. Xu, C. Jiang, X. Lu, J. Fan and M. Gu, J. Mater. Chem. A, 2019, 7, 2780-2786.